



## Inter-annual variability of the global terrestrial water cycle

Dongqin Yin<sup>1,2</sup>, Michael L. Roderick<sup>1,2,3</sup>

<sup>1</sup>Research School of Earth Sciences, Australian National University, Canberra, ACT, 2601, Australia

<sup>2</sup>Australian Research Council Centre of Excellence for Climate System Science, Canberra, ACT, 2601, Australia

<sup>3</sup>Australian Research Council Centre of Excellence for Climate Extremes, Canberra, ACT, 2601, Australia

Correspondence to: ([dongqin.yin@anu.edu.au](mailto:dongqin.yin@anu.edu.au))

### Abstract:

1 Variability of the terrestrial water cycle, i.e., precipitation ( $P$ ), evapotranspiration ( $E$ ), runoff ( $Q$ ) and water storage  
2 change ( $\Delta S$ ) is the key to understanding hydro-climate extremes. However, a comprehensive global assessment  
3 for the partitioning of variability in  $P$  between  $E$ ,  $Q$  and  $\Delta S$  is still not available. In this study, we use the recently  
4 released global monthly hydrologic reanalysis product known as the Climate Data Record (CDR) to conduct an  
5 initial investigation of the inter-annual variability of the global terrestrial water cycle. We first examine global  
6 patterns in partitioning the long-term mean  $\bar{P}$  between the various sinks  $\bar{E}$ ,  $\bar{Q}$  and  $\bar{\Delta S}$  and confirm the well-known  
7 patterns with  $\bar{P}$  partitioned between  $\bar{E}$  and  $\bar{Q}$  according to the aridity index. In a new analysis based on the concept  
8 of variability source and sinks (Eq. 2) we then examine how variability in the precipitation  $\sigma_P^2$  (the source) is  
9 partitioned between the three variability sinks  $\sigma_E^2$ ,  $\sigma_Q^2$  and  $\sigma_{\Delta S}^2$  along with the three relevant covariance terms, and  
10 how that partitioning varies with the aridity index. We find that the partitioning of inter-annual variability does  
11 not simply follow the mean state partitioning, with  $\sigma_P^2$  mostly partitioned between  $\sigma_Q^2$ ,  $\sigma_{\Delta S}^2$  and the associated  
12 covariances. We also find that the magnitude of the covariance components can be large and often negative,  
13 indicating the variability in the sinks (e.g.,  $\sigma_Q^2$ ,  $\sigma_{\Delta S}^2$ ) can, and do, exceed variability in the source ( $\sigma_P^2$ ). Further  
14 investigations under extreme conditions reveal that in extremely dry environments the variance partitioning is  
15 closely related to the water storage capacity. With limited storage capacity the partitioning of  $\sigma_P^2$  is mostly to  $\sigma_E^2$ ,  
16 but as the storage capacity increases the partitioning of  $\sigma_P^2$  is increasingly shared between  $\sigma_E^2$ ,  $\sigma_{\Delta S}^2$  and the  
17 covariance between those variables. In other environments (i.e., extremely wet and semi-arid/semi-humid) the  
18 variance partitioning proved to extremely complex and a synthesis was not developed. We anticipate that a major  
19 scientific effort will be needed to develop a synthesis of hydrologic variability.

20

21



## 22 1. Introduction

23

24 In describing the terrestrial branch of the water cycle, the precipitation ( $P$ ) is partitioned into evapotranspiration  
25 ( $E$ ), runoff ( $Q$ ) and change in water storage ( $\Delta S$ ). With averages taken over many years,  $\overline{\Delta S}$  is usually assumed to  
26 be zero and it has long been recognized that the partitioning of the long-term mean annual precipitation ( $\overline{P}$ )  
27 between  $\overline{E}$  and  $\overline{Q}$  was jointly determined by the availability of both water ( $\overline{P}$ ) and energy (represented by the net  
28 radiation expressed as an equivalent depth of water and denoted  $\overline{E}_o$ ) fluxes. Using data from a large number of  
29 watersheds, Budyko (1974) developed an empirical relation relating the evapotranspiration ratio ( $\overline{E}/\overline{P}$ ) to the  
30 aridity index ( $\overline{E}_o/\overline{P}$ ). The resultant empirical relation and other Budyko-type forms (e.g., Fu, 1981; Choudhury,  
31 1999; Yang et al., 2008, Roderick and Farquhar, 2011; Sposito, 2017) that partition  $P$  between  $E$  and  $Q$  have  
32 proven to be extremely useful in both understanding and characterising the long-term mean annual hydrological  
33 conditions in a given region.

34

35 However, the long-term mean annual hydrologic fluxes rarely occur in any given year. Instead, society must  
36 (routinely) deal with variability around the long-term mean. The classic hydro-climate extremes are droughts and  
37 floods but the key point here is that hydrologic variability is expressed on a full spectrum of time and space scales.  
38 To accommodate that perspective, we need to extend our thinking beyond the long-term mean to ask how the  
39 variability of  $P$  is partitioned into the variability of  $E$ ,  $Q$  and  $\Delta S$ ?

40

41 Early research on hydrologic variability focussed on extending the Budyko curve. In particular, Koster and Suarez  
42 (1999) used the Budyko curve to analyse inter-annual variability in the water cycle. In their framework, the  
43 evapotranspiration standard deviation ratio (defined as the ratio of standard deviation for  $E$  to  $P$ ,  $\sigma_E/\sigma_P$ ) was (also)  
44 estimated using the aridity index ( $\overline{E}_o/\overline{P}$ ). The classic Koster and Suarez framework has been widely applied and  
45 extended in investigations of the variability in both  $E$  and  $Q$ , using catchment observations, reanalysis data and  
46 model outputs (e.g., McMahon et al., 2011; Wang and Alimohammadi 2012; Sankarasubramanian and Vogel,  
47 2002; Zeng and Cai, 2015). However, typical applications of the Koster and Suarez framework have previously  
48 been at regional scales and there is still no comprehensive global assessment for the partitioning of variability of  
49  $P$  into the variability of  $E$ ,  $Q$  and  $\Delta S$ . One reason for the lack of a global comprehensive assessment is the absence  
50 of gridded global hydrologic data. Interestingly, the atmospheric science community have long used a



51 combination of observations and model outputs to construct global atmospheric re-analyses and such products  
52 have become central to atmospheric research. Those atmospheric products also contain estimates of some of the  
53 key water cycle variables (e.g.,  $P$ ,  $E$ ), such as in the widely used interim ECMWF Re-Analysis (ERA-Interim;  
54 Dee et al. 2011). However, the central aim of atmospheric re-analysis is to estimate atmospheric variables, which,  
55 understandably, ignores many of the nuances of soil water infiltration, vegetation water uptake, runoff generation  
56 and many other processes of central importance in hydrology.

57

58 Hydrologists have only recently accepted the challenge of developing their own re-analysis type products with  
59 perhaps the first serious hydrologic re-analysis being published as recently as a few years ago (Rodell et al., 2015).  
60 More recently, the Princeton University group has extended this early work by making available a gridded global  
61 terrestrial hydrologic re-analysis product known as the Climate Data Record (CDR) (Zhang et al., 2018). Briefly,  
62 the CDR was constructed by synthesizing multiple in-situ observations, satellite remote sensing products, and  
63 land surface model outputs to provide *gridded* estimates of global land precipitation  $P$ , evapotranspiration  $E$ ,  
64 runoff  $Q$  and total water storage change  $\Delta S$  ( $0.5^\circ \times 0.5^\circ$ , monthly, 1984-2010). In developing the CDR, the authors  
65 adopted local water budget closure as the fundamental hydrologic principle. That approach presented one  
66 important difficulty. Global observations of  $\Delta S$  start with the GRACE satellite mission from 2002. Hence before  
67 2002 there is no direct observational constraint on  $\Delta S$  and the authors made the further assumption that the mean  
68 annual  $\Delta S$  over the full 1984-2010 period was zero at every grid-box. That is incorrect in some regions (e.g.  
69 Scanlon et al., 2018) and represents an observational problem that cannot be overcome. However, our interest is  
70 in the year-to-year variability and for that application, the assumption of no change in the mean annual  $\Delta S$  over  
71 the full 1984-2010 period is unlikely to lead to major problems since we are not looking for subtle changes over  
72 the full time series. With that caveat in mind, the aim of this study is to use this new 27-year gridded hydrologic  
73 re-analysis product to conduct an initial investigation of the inter-annual variability of the terrestrial branch of the  
74 global water cycle.

75

76 The paper is structured as follows. We begin in Section 2 by describing the various climate and hydrologic  
77 databases including a further assessment of the suitability of the CDR database for this initial variability study. In  
78 Section 3, we examine relationships between the mean and variability in the four water cycle variables ( $P$ ,  $E$ ,  $Q$   
79 and  $\Delta S$ ). In Section 4, we first relate the variability to classical aridity index and then use those results to evaluate



80 the theory of Koster and Suarez (1999). Subsequently we examine how the variance of  $P$  is partitioned into the  
81 variances (and relevant covariances) of  $E$ ,  $Q$  and  $\Delta S$  and investigate some factors controlling the variance  
82 partitioning. We finalise the paper with a discussion summarising what we have learnt about water cycle  
83 variability over land by using the CDR database.

84

## 85 2. Methods and Data

### 86 2.1 Methods

87 The water balance is defined by,

$$88 \quad P(t) = E(t) + Q(t) + \Delta S(t) \quad (1)$$

89 with  $P$  the precipitation,  $E$  the evapotranspiration,  $Q$  the runoff and  $\Delta S$  the total water storage change in time  
90 step  $t$ . By the usual variance law, we have,

$$91 \quad \sigma_P^2 = \sigma_E^2 + \sigma_Q^2 + \sigma_{\Delta S}^2 + 2cov(E, Q) + 2cov(E, \Delta S) + 2cov(Q, \Delta S) \quad (2)$$

92 that includes all relevant variances (denoted  $\sigma^2$ ) and covariances (denoted  $cov$ ). Eq. (1) is the familiar  
93 hydrologic mass balance equation. In that context, Eq. (2) can be thought of as the hydrologic variance balance  
94 equation.

95

### 96 2.2 Hydrologic and Climatic Data

97

98 We use the recently released global land hydrologic re-analysis known here as the Climate Data Record (CDR)  
99 (Zhang et al., 2018). This product includes global precipitation  $P$ , evapotranspiration  $E$ , runoff  $Q$  and water storage  
100 change  $\Delta S$  ( $0.5^\circ \times 0.5^\circ$ , monthly, 1984-2010). The CDR does not report additional radiative variables and we use  
101 the NASA/GEWEX Surface Radiation Budget (SRB) Release-3.0 (monthly, 1984-2007,  $1^\circ \times 1^\circ$ ) database  
102 (Stackhouse et al., 2011) to calculate  $E_o$  (defined as the net radiation expressed as an equivalent depth of liquid  
103 water, Budyko, 1974). We then calculate the aridity index ( $\overline{E_o}/\overline{P}$ ) using  $P$  from the CDR and  $E_o$  from the SRB  
104 databases (see Fig. S1a in the Supplementary Material).

105

106 On general grounds, we anticipate that two important factors likely to control the partitioning of hydrologic  
107 variability were the water storage capacity and the presence of ice/snow at the surface. For the storage, we estimate  
108 the water storage capacity ( $S_{\max}$ ) using the monthly  $\Delta S$  data in CDR database. The water storage  $S(t)$  at each time



109 step  $t$  (monthly here) was first calculated from the accumulation of  $\Delta S(t)$ , i.e.,  $S(t) = S(t-1) + \Delta S(t)$  where we  
110 assumed zero storage at the beginning of the study period (i.e.,  $S(0) = 0$ ). With the resulting time series available,  
111  $S_{\max}$  was estimated as the difference between the maximum and minimum  $S(t)$  during the study period at each  
112 grid-box (see Fig. S1b in the Supplementary Material). The estimated  $S_{\max}$  shows a large range from 0 to 1000  
113 mm with the majority of values from 50 to 600 mm (Fig. S1b), which generally agrees with global rooting depth  
114 estimates assuming that water occupies from 10 to 30% of the soil volume at field capacity (Jackson et al., 1996;  
115 Wang-Erlandsson et al., 2016; Yang et al., 2016). To characterise snow/ice cover, and to distinguish extremely  
116 hot and cold regions, we also make use of a gridded global land air temperature dataset from the Climatic Research  
117 Unit (CRU TS4.01 database, monthly, 1901-2016,  $0.5^\circ \times 0.5^\circ$ ) (Harris et al., 2014). (see Fig. S1c in the  
118 Supplementary Material).

119

### 120 2.3 Spatial Mask to Define Study Extent

121

122 The CDR database provides an estimate of the uncertainty ( $\pm 1\sigma$ ) for each of the hydrologic variables ( $P$ ,  $E$ ,  $Q$ ,  
123  $\Delta S$ ) in each month. We use those uncertainty estimates to identify and remove regions with high relative  
124 uncertainty in the CDR data. The relative uncertainty is calculated as the ratio of root mean square of the  
125 uncertainty ( $\pm 1\sigma$ ) to the mean annual  $P$ ,  $E$  and  $Q$  at each grid-box following the procedure used by Milly and  
126 Dunne (2002a). Note that the long term mean  $\Delta S$  is zero by construction in the CDR database, and for that reason  
127 we did not use  $\Delta S$  to calculate the relative uncertainty. Grid-boxes with a relative uncertainty (in  $P$ ,  $E$  and  $Q$ ) more  
128 than 0.1 are deemed to have high relative uncertainty (Milly and Dunne, 2002a) and were excluded from the study  
129 extent. The excluded grid-boxes were mostly in the Himalayan region, the Sahara Desert and in Greenland. The  
130 final spatial mask is shown in Fig. 1 and this has been applied throughout this study.

131

### 132 2.4 Further Evaluation of CDR Data for Variability Analysis

133

134 In the original work, the CDR database was validated by comparison with independent observations including (i)  
135 mean seasonal cycle of  $Q$  from 26 large basins (see Fig. 8 in Zhang et al., 2018), (ii) mean seasonal cycle of  $\Delta S$   
136 from 12 large basins (Fig. 10 in Zhang et al., 2018), (iii) monthly runoff from 165 medium size basins and a  
137 further 862 small basins (Fig. 14 in Zhang et al., 2018), (iv) summer  $E$  from 47 flux towers (Fig. 16 in Zhang et  
138 al., 2018). Those evaluations did not directly address variability in various water cycle elements. With our focus



139 on the variability we decided to conduct further validations of the CDR database beyond those described in the  
140 original work. In particular, we focussed on further independent assessments of  $E$  and we use monthly (as opposed  
141 to summer) observations of  $E$  from FLUXNET to evaluate the variability in  $E$ . We also compare the CDR with  
142 two other gridded global  $E$  products that were not used to develop the CDR including LandFluxEval ( $1^\circ \times 1^\circ$ ,  
143 monthly, 1989-2005) (Mueller et al., 2013) and the Max Planck Institute (MPI,  $0.5^\circ \times 0.5^\circ$ , monthly, 1982-2011)  
144 (Jung et al., 2010) product.

145

146 For the comparison to FLUXNET observations (Baldocchi et al., 2001; Agarwal et al., 2010) we identified 32  
147 flux tower sites (site locations are shown in Fig. S2 and details are shown in Table S1) having at least three years  
148 of continuous (monthly) measurements using the FluxnetLSM R package (v1.0) (Ukkola et al. 2017). The monthly  
149 totals and annual climatology of  $P$  and  $E$  from CDR generally follow FLUXNET observations, with high  
150 correlations and reasonable Root Mean Square Error (Figs. S3-S4, Table S1). Comparison of the point-based  
151 FLUXNET ( $\sim 100$  m – 1 km scale) with the grid-based CDR ( $\sim 50$  km scale) is problematic since the CDR  
152 represents an area that is at least 2500 times larger than the area represented by the individual FLUXNET towers  
153 and we anticipate that the CDR record would be “smoothed” relative to the FLUXNET record. With that in mind,  
154 we chose to compare the ratio of the standard deviation of  $E$  to  $P$  between the CDR and FLUXNET databases and  
155 this normalised comparison of the hydrologic variability proved encouraging (Fig. S5).

156

157 As a further evaluation, we compare gridded  $E$  data in the CDR database against two other global  $E$  databases  
158 including LandFluxEVAL ( $1^\circ \times 1^\circ$ , monthly, 1989-2005) (Mueller et al., 2013) and Max Planck Institute (MPI,  
159  $0.5^\circ \times 0.5^\circ$ , monthly, 1982-2011) (Jung et al., 2010) that were not used to construct the CDR database. We found  
160 that monthly mean  $E$  from the CDR database is slightly underestimated compared with LandFluxEVAL database  
161 (Fig. S6a), but agrees closely with the MPI database (Fig. S7a). In terms of variability, the standard deviations of  
162 monthly  $E$  from the CDR are slightly different than those in the MPI database (Fig. S7c) but were in very close  
163 agreement with the LandFluxEVAL database (Fig. S6c).

164

165 In summary, we concluded that the CDR database was suitable for an initial investigation of the inter-annual  
166 variability in the water cycle.

167

168 **3. Mean and Variability of Water Cycle Components**

169 3.1 Mean Annual  $P$ ,  $E$ ,  $Q$  and the Budyko Curve

170

171 The global pattern of mean annual  $P$ ,  $E$ ,  $Q$  using the CDR data (1984-2007) is shown in Fig. 2. The mean annual  
172  $P$  ( $\bar{P}$ ) is prominent in tropical regions, southern China, eastern and western North America (Fig. 2a). The  
173 magnitude of mean annual  $E$  ( $\bar{E}$ ) more or less follows the pattern of  $\bar{P}$  in the tropics (Fig. 2b) while the mean  
174 annual  $Q$  ( $\bar{Q}$ ) is particularly prominent in the Amazon, South and Southeast Asia, tropical parts of west Africa  
175 and in some other coastal regions at higher latitudes (Fig. 2c).

176

177 We relate the grid-box level ratio of  $\bar{E}$  to  $\bar{P}$  in the CDR database to the classical Budyko (1974) curve using the  
178 aridity index ( $\bar{E}_o/\bar{P}$ ) (Fig. 3a). As noted previously, in the CDR database,  $\bar{\Delta S}$  is forced to be zero and this enforced  
179 steady state allowed us to also predict the ratio of  $\bar{Q}$  to  $\bar{P}$  using the same Budyko curve (Fig. 3b). The Budyko  
180 curves follow the overall trend in the CDR data. However, there is substantial scatter due to, for example, regional  
181 variations related to seasonality, water storage change and physics of runoff generation (Milly, 1994a, b). The  
182 overall patterns are as expected with  $\bar{E}$  following  $\bar{P}$  in dry environments ( $\bar{E}_o/\bar{P} > 1.0$ ) while  $\bar{E}$  follows  $\bar{E}_o$  in wet  
183 environments ( $\bar{E}_o/\bar{P} \leq 1.0$ ) (Fig. 3).

184

185 3.2 Inter-annual Variability in  $P$ ,  $E$ ,  $Q$  and  $\Delta S$ 

186

187 We use the variance balance equation (Eq. 2) to partition the inter-annual  $\sigma_P^2$  into separate components due to  $\sigma_E^2$ ,  
188  $\sigma_Q^2$ ,  $\sigma_{\Delta S}^2$  along with the three covariance components ( $2cov(E, Q)$ ,  $2cov(E, \Delta S)$ ,  $2cov(Q, \Delta S)$ ) (Fig. 4). The  
189 spatial pattern of  $\sigma_P^2$  (Fig. 4a) is very similar to that of  $\bar{P}$  (Fig. 2a), which implies that the  $\sigma_P^2$  is positively  
190 correlated with  $\bar{P}$ . In contrast the partitioning of  $\sigma_P^2$  to the various components is very different from the  
191 partitioning of  $\bar{P}$  (cf. Fig. 2 and 4). First we note that while the overall spatial pattern of  $\sigma_E^2$  more or less follows  
192  $\sigma_P^2$ , the overall magnitude of  $\sigma_E^2$  is much smaller than  $\sigma_P^2$  and  $\sigma_Q^2$  in most regions, and in fact  $\sigma_E^2$  is also generally  
193 smaller than  $\sigma_{\Delta S}^2$ . The prominence of  $\sigma_{\Delta S}^2$  (compared to  $\sigma_E^2$ ) surprised us. The three covariance components  
194 ( $cov(E, Q)$ ,  $cov(E, \Delta S)$ ,  $cov(Q, \Delta S)$ ) are also important in some regions. In more detail, the  $cov(E, Q)$  term is  
195 prominent in regions where  $\sigma_Q^2$  is large and is mostly negative in those regions (Fig. 4e), indicating that years with  
196 lower  $E$  are associated with higher  $Q$  and vice-versa. There are also a few regions with prominent positive values  
197 for  $cov(E, Q)$  (e.g., the seasonal hydroclimates of northern Australia) indicating that in those regions, years with  
198 a higher  $E$  are associated with higher  $Q$ . The  $cov(E, \Delta S)$  term (Fig. 4f) has a similar spatial pattern to the



199  $cov(E, Q)$  term (Fig. 4e) but with a smaller overall magnitude. Finally, the  $cov(Q, \Delta S)$  term shows a more  
200 complex spatial pattern, with both prominent positive and negative values (Fig. 4g) in regions where  $\sigma_Q^2$  (Fig. 4c)  
201 and  $\sigma_{\Delta S}^2$  (Fig. 4d) are both large.

202

203 These results show that the spatial patterns in variability are not simply a reflection of patterns in the long-term  
204 mean state. On the contrary, we find that of the three primary variance terms, the overall magnitude of (inter-  
205 annual)  $\sigma_E^2$  is the smallest implying the least (inter-annual) variability in  $E$ . This is very different from the  
206 conclusions based on spatial patterns in the mean  $P$ ,  $E$  and  $Q$  (see previous section). Further, while  $\sigma_Q^2$  more or  
207 less follows  $\sigma_P^2$  as expected, we were surprised by the magnitude of  $\sigma_{\Delta S}^2$  which, in general, substantially exceeds  
208 the magnitude of  $\sigma_E^2$ . Further, the magnitude of the covariance terms can be important, especially in regions with  
209 high  $\sigma_Q^2$ . However, unlike the variances, the covariance can be both positive and negative and this introduces  
210 additional complexity. For example, with a negative covariance it is possible for the variance in  $Q$  ( $\sigma_Q^2$ ) to exceed  
211 the variance in  $P$  ( $\sigma_P^2$ ). To examine that in more detail we calculated the equivalent frequency distribution for each  
212 of the plots in Fig. 4. The results (Fig. 5) further emphasise that in general,  $\sigma_E^2$  is the smallest of the variances (Fig.  
213 5b). We also note that the frequency distributions for the covariances (Fig. 5efg) are not symmetrical. In summary,  
214 it is clear that spatial patterns in the inter-annual variability of the water cycle (Fig. 4) do not simply follow the  
215 spatial patterns for the inter-annual mean (Fig. 2).

216

### 217 3.3 Relation Between Variability and the Mean State for $P$ , $E$ , $Q$

218

219 Differences in the spatial patterns of the mean (Fig. 2) and inter-annual variability (Fig. 4) in the global water  
220 cycle led us to further investigate the relation between the mean and the variability for each separate component.  
221 Here we relate the standard deviation ( $\sigma_P$ ,  $\sigma_E$ ,  $\sigma_Q$ ) instead of the variance to the mean of each water balance flux  
222 (Fig. 6) since the standard deviation has the same physical units as the mean making the results more comparable.  
223 As inferred previously, we find  $\sigma_P$  to be positively correlated with  $\bar{P}$  but with substantial scatter (Fig. 6a). The  
224 same result more or less holds for the relation between  $\sigma_Q$  and  $\bar{Q}$  (Fig. 6c). In contrast the relation between  $\sigma_E$  and  
225  $\bar{E}$  is very different (Fig. 6b). In particular,  $\sigma_E$  is a small fraction of  $\bar{E}$  and this complements the earlier finding (Fig.  
226 6b) that the inter-annual variability for  $E$  is generally smaller than for the other physical variables,  $P$ ,  $Q$  or  $\Delta S$ .  
227 (The same result was also found using both LandFluxEVAL and MPI databases, see Fig. S8 in the Supplementary  
228 Material.) Importantly, unlike  $P$  and  $Q$ ,  $E$  is constrained by both water and energy availability (Budyko, 1974)





229 and the limited inter-annual variability in  $E$  presumably reflects limited inter-annual variability in the available  
230 (radiant) energy ( $E_o$ ). This is something that could be investigated in a future study.

231

#### 232 4. Relating the Variability of $P$ , $E$ , $Q$ and $\Delta S$ to Aridity

233

234 In the previous section, we investigated spatial patterns of the mean and the variability in the global water cycle.

235 In this section, we extend that by investigating the partitioning of  $\sigma_p^2$  to the three primary physical terms ( $\sigma_E^2$ ,  $\sigma_Q^2$ ,

236  $\sigma_{\Delta S}^2$ ) along with the three relevant covariances. For that, we begin by comparing the Koster and Suarez (1999)

237 theory against the CDR data and then investigate how the partitioning of the variance is related to the aridity index

238  $\overline{E_o}/\overline{P}$  (see Fig. S1a in the Supplementary Material). Following that, we investigate variance partitioning in relation

239 to both our estimate of the storage capacity  $S_{\max}$  (see Fig. S1b in the Supplementary Material) as well as the mean

240 annual air temperature  $\overline{T_a}$  (see Fig. S1c in the Supplementary Material) that we use as a surrogate for snow/ice

241 cover. We finalise this section by examining the partitioning of variance at three selected study sites that represent

242 extremely dry/wet, high/low water storage capacity and the hot/cold spectrums.

243

##### 244 4.1 Comparison with the Koster and Suarez (1999) Theory

245

246 We first evaluate the classical empirical curve of Koster and Suarez (1999) by relating ratios  $\sigma_E/\sigma_p$  and  $\sigma_Q/\sigma_p$  to

247 the aridity index (Fig. 7). The ratio  $\sigma_E/\sigma_p$  in the CDR database is generally overestimated by the empirical Koster

248 and Suarez curve, especially in dry environments (e.g.,  $\overline{E_o}/\overline{P} > 3$ ). The inference here is that the Koster and Suarez

249 theory predicts  $\sigma_E/\sigma_p$  to approach unity in dry environments while the equivalent value in the CDR data is

250 occasionally unity but is generally smaller. With  $\sigma_E/\sigma_p$  generally overestimated by the Koster and Suarez theory

251 we expect, and find, that  $\sigma_Q/\sigma_p$  is underestimated by the same theory (Fig. 7b). The same overestimation was

252 found based on the other two independent databases for  $E$  (LandFluxEVAL and MPI) (Fig. S9). This

253 overestimation is discussed further in section 5.

254

##### 255 4.2 Relating Inter-annual Variability to Aridity

256

257 Here we examine how the fraction of the total variance in precipitation accounted for by the three primary variance

258 terms along with the three covariance terms varies with the aridity index ( $\overline{E_o}/\overline{P}$ ) (Fig. 8). (Also see Fig. S10 for



259 the spatial maps.) The ratio  $\sigma_E^2/\sigma_P^2$  is close to zero in extremely wet regions and has an upper limit noted  
260 previously (Fig. 7a) that approaches unity in extremely dry regions (Fig. 8a). The ratio  $\sigma_Q^2/\sigma_P^2$  is close to zero in  
261 extremely dry regions but approaches unity in extremely wet regions but with substantial scatter (Fig. 8b). The  
262 ratio  $\sigma_{\Delta S}^2/\sigma_P^2$  is close to zero in both extremely dry/wet regions (Fig. 8c) but shows the largest range at an  
263 intermediate aridity index ( $\overline{E_o}/\overline{P} \sim 1.0$ ).

264

265 The covariance ratios are all small in extremely dry (e.g.,  $\overline{E_o}/\overline{P} \geq 6.0$ ) environments and generally show the largest  
266 range in semi-arid and humid environments. The peak magnitudes for the three covariance components  
267 consistently occur when  $\overline{E_o}/\overline{P}$  is close to 1.0 which is the threshold often used to separate wet and dry  
268 environments.

269

#### 270 4.3 Further Investigations on the Factors Controlling Partitioning of the Variance

271

272 The previous results (Sections 4.1 and 4.2) have demonstrated that spatial variation in the partitioning of  $\sigma_P^2$  into  
273  $\sigma_E^2$ ,  $\sigma_Q^2$ ,  $\sigma_{\Delta S}^2$  and the three covariance components is complex. To help further understand inter-annual variability  
274 of the terrestrial water cycle, we conduct further investigations in this section using two factors likely to have a  
275 major influence on the variance partitioning of  $\sigma_P^2$ . The first is the storage capacity  $S_{\max}$  (see Fig. S1b in the  
276 Supplementary Material). The second is the mean annual air temperature  $\overline{T_a}$  (see Fig. S1c in the Supplementary  
277 Material) which is used here as a surrogate for snow/ice presence.

278

##### 279 4.3.1 Relating Inter-annual Variability to Storage Capacity

280

281 We first relate the partitioning of  $\sigma_P^2$  to water storage capacity ( $S_{\max}$ ) by repeating Fig. 8 but instead we use a  
282 logarithmic scale for the x-axis and we distinguish  $S_{\max}$  via the background colour (Fig. 9). To eliminate the  
283 possible overlap of grid-cells in the colouring process, all the grid-cells over land are further separated using  
284 different latitude ranges (as shown in the four columns of Fig. 9), i.e., 90N-60N, 60N-30N, 30N-0 and 0-90S. We  
285 find that  $S_{\max}$  is relatively high in wet environments ( $\overline{E_o}/\overline{P} \leq 1.0$ ) but shows no obvious relation with the  
286 partitioning of  $\sigma_P^2$ . However, in dry environments ( $\overline{E_o}/\overline{P} > 1.0$ ) the ratio  $\sigma_E^2/\sigma_P^2$  apparently decreases with the  
287 increase of  $S_{\max}$  (Fig. 9a-d). That relation is particularly obvious in extremely dry environments ( $\overline{E_o}/\overline{P} \geq 6.0$ ) at  
288 equatorial latitudes where there is an upper limit of  $\sigma_E^2/\sigma_P^2$  close to 1.0 when  $S_{\max}$  is small (blue grid-cells in Fig.



289 9c). The interpretation for those extremely dry environments is that when  $S_{\max}$  is small,  $\sigma_P^2$  is almost completely  
290 partitioned into  $\sigma_E^2$  (Fig. 9bc) with the other variance and covariance components close to zero. While for those  
291 same extremely dry environments, as  $S_{\max}$  increases, the partitioning of  $\sigma_P^2$  is shared between  $\sigma_E^2$  and  $\sigma_{\Delta S}^2$  and their  
292 covariance (Fig. 9cks) with  $\sigma_Q^2$  and its covariance components close to zero (Fig. 9gow). However, at polar  
293 latitudes in the northern hemisphere (panels in the first and second columns of Fig. 9) there are variations that  
294 could not be easily associated with variations in  $S_{\max}$  which led us to investigate the role of snow/ice on the  
295 variance partitioning in the following section.

296

#### 297 4.3.2 Relating Inter-annual Variability to Mean Air Temperature

298

299 To understand the potential role of snow/ice in modifying the variance partitioning, we repeat the previous  
300 analysis (Fig. 9) but here we use the mean annual air temperature ( $\overline{T_a}$ ) to colour the grid-cells to crudely identify  
301 the presence of snow/ice (Fig. 10). Most of the variations at polar latitudes in the northern hemisphere (panels in  
302 the first and second columns of Fig. 10) is associated with low air temperature (e.g.,  $\overline{T_a} < 0$  °C in blue colour),  
303 making the results associated with high air temperature (e.g.,  $\overline{T_a} > 10$  °C in green-yellow-red colours) relatively  
304 more compact. That pattern is particularly obvious in extremely wet environment, where the ratio  $\sigma_Q^2/\sigma_P^2$  is close  
305 to 1.0 when  $\overline{T_a}$  is high (e.g.,  $\overline{E_o}/\overline{P} \leq 0.5$  and  $\overline{T_a} > 10$  °C, with green-yellow-red grid-cells on the panels in the  
306 second row of Fig. 10) with the other variance-covariance components close to zero. This indicates that in  
307 extremely wet environment, when  $\overline{T_a}$  is high,  $\sigma_P^2$  is almost completely partitioned into  $\sigma_Q^2$ . However, when  $\overline{T_a}$  is  
308 low in extremely wet environment, there are substantial variations in all variance-covariance components  
309 (e.g.,  $\overline{E_o}/\overline{P} \leq 0.5$  and  $\overline{T_a} < 0$  °C, see the blue grid-cells on the panels in the first column of Fig. 10). That result  
310 indicates the complexity of variance partitioning associated with the presence of snow/ice.

311

#### 312 4.4 Case Studies

313

314 The previous results (Section 4.3) have demonstrated that the partitioning of  $\sigma_P^2$  is predominantly influenced by  
315 the water storage capacity ( $S_{\max}$ ) in extremely dry environments ( $\overline{E_o}/\overline{P} \geq 6.0$ ) and by mean air temperature ( $\overline{T_a}$ )  
316 in extremely wet environments ( $\overline{E_o}/\overline{P} \leq 0.5$ ). In this section, we examine, in greater detail, several sites to gain  
317 deeper understanding of the partitioning of  $\sigma_P^2$ . For that purpose, we selected three sites based on extreme values  
318 for the three explanatory parameters, i.e.,  $\overline{E_o}/\overline{P}$  (Fig. S1a),  $S_{\max}$  (Fig. S1b) and  $\overline{T_a}$  (Fig. S1c). The criteria to select



319 three climate sites are as follows, Site 1: dry ( $\overline{E_o}/\overline{P} \geq 6.0$ ) and small  $S_{\max}$  ( $S_{\max} \approx 0$ ), Site 2: dry ( $\overline{E_o}/\overline{P} \geq 6.0$ ) and  
320 relatively large  $S_{\max}$  ( $S_{\max} \gg 0$ ) and Site 3: wet ( $\overline{E_o}/\overline{P} \leq 0.5$ ) and hot ( $\overline{T_a} > 25$  °C). For each of the three sites, we  
321 use a representative grid-cell (Fig. 11) to show the original time series (Fig. 12) and the partitioning of variability  
322 (Fig. 13).

323

324 We show the  $P$ ,  $E$ ,  $Q$  and  $\Delta S$  time series along with the relevant variances and covariances in Fig. 12. Starting  
325 with the two dry sites, at the site with low storage capacity (Site 1), the time series shows that  $E$  closely follows  
326  $P$  leaving annual  $Q$  and  $\Delta S$  close to zero (Fig. 12a). The variance of  $P$  ( $\sigma_P^2 = 206.9$  mm<sup>2</sup>) is small and almost  
327 completely partitioned into the variance of  $E$  ( $\sigma_E^2 = 196.9$  mm<sup>2</sup>), leaving very limited variance for  $Q$ ,  $\Delta S$  and all  
328 three covariance components (Fig. 12b). At the site with high storage capacity (Site 2),  $E$ ,  $Q$  and  $\Delta S$  do not simply  
329 follow  $P$  (Fig. 12c). As a consequence, the variance of  $P$  ( $\sigma_P^2 = 2798.0$  mm<sup>2</sup>) is shared between  $E$  ( $\sigma_E^2 = 1150.2$   
330 mm<sup>2</sup>),  $\Delta S$  ( $\sigma_{\Delta S}^2 = 800.5$  mm<sup>2</sup>) and their covariance component ( $2cov(E, \Delta S) = 538.4$  mm<sup>2</sup>, Fig. 12d). Switching  
331 now to the remaining wet and hot site (Site 3),  $Q$  closely follows  $P$ , with  $\Delta S$  close to zero and  $E$  showing little  
332 inter-annual variation (Fig. 12e). The variance of  $P$  ( $\sigma_P^2 = 57374.4$  mm<sup>2</sup>) is relatively large and almost completely  
333 partitioned into the variance of  $Q$  ( $\sigma_Q^2 = 57296.4$  mm<sup>2</sup>), leaving very limited variance for  $E$  and  $\Delta S$  and the three  
334 covariance components (Fig. 12f). We also examined numerous other sites with similar extreme conditions as the  
335 three case study sites and found the same basic patterns as reported above.

336

337 To put the data from the three case study sites into a broader variability context we position the site data onto a  
338 backdrop of original Fig. 8. As noted previously, at Site 1, the ratio  $\sigma_E^2/\sigma_P^2$  is very close to unity (Fig. 13a), and  
339 under this extreme condition, we have the following approximation,

$$340 \quad \sigma_P^2 \approx \sigma_E^2 \quad (\text{Site 1, dry and } S_{\max} \approx 0) \quad (3)$$

341 In contrast, for Site 2 with the same aridity index but higher  $S_{\max}$ , we have,

$$342 \quad \sigma_P^2 \approx \sigma_E^2 + \sigma_{\Delta S}^2 + 2cov(E, \Delta S) \quad (\text{Site 2, dry and } S_{\max} \gg 0) \quad (4)$$

343 Finally, at Site 3, we have,

$$344 \quad \sigma_P^2 \approx \sigma_Q^2 \quad (\text{Site 3, wet and hot}) \quad (5)$$

345

346 4.5 Synthesis

347



348 The above simple examples demonstrate that aridity  $\overline{E_o}/\overline{P}$ , storage capacity  $S_{\max}$  and air temperature  $\overline{T_a}$  all play  
349 roles in the partitioning of  $\sigma_P^2$  to the various components. Our synthesis of the results for the partitioning of  $\sigma_P^2$  is  
350 summarised in Fig. 14. In dry and  $S_{\max} \approx 0$  environments we have minimal runoff and expect that  $\sigma_P^2$  is more or  
351 less completely partitioned into  $\sigma_E^2$  (Fig. 14a). In those environments, (inter-annual) variations in storage  $\sigma_{\Delta S}^2$  play  
352 a limited role in setting the overall variability. However, in dry and  $S_{\max} \gg 0$  environments,  $\sigma_E^2$  is only a fraction  
353 of  $\sigma_P^2$  leaving the overall variance attributed to  $\sigma_{\Delta S}^2$  and the covariance between  $E$  and  $\Delta S$  (Fig. 14c and Fig. 14e).  
354 This implies the hydrological importance of water storage capacity in buffering variations of the water cycle under  
355 dry conditions.

356

357 Under extremely wet conditions, the huge difference in variance partitioning occurs between the hot and cold  
358 conditions instead of water storage capacity conditions in dry conditions. In wet and hot environments, we have  
359 maximum runoff and expect that  $\sigma_P^2$  is more or less completely partitioned into  $\sigma_Q^2$  (Fig. 14b), and the variations  
360 in evapotranspiration  $\sigma_E^2$  and storage  $\sigma_{\Delta S}^2$  play a limited role in setting the overall variability. However, in wet and  
361 cold environments, the variance partitioning shows great complexity, with  $\sigma_Q^2/\sigma_P^2$  and  $\sigma_{\Delta S}^2/\sigma_P^2$  vary a lot caused  
362 by snow/ice melting. This signifies the hydrological importance of thermal processes (melting/freezing) under  
363 extremely cold conditions.

364

365 The most complex patterns to interpret are those for semi-arid to semi-humid environments (i.e.,  $\overline{E_o}/\overline{P} \sim 1.0$ ). In  
366 those environments, the three covariance terms all play important roles and we found that simple environmental  
367 gradients (e.g., dry/wet, high/low storage capacity, hot/cold) could not easily explain the observed patterns. A  
368 major effort will be needed to discover the controlling factors for variability of the water cycle in these  
369 environments.

370

## 371 5. Discussion

372

373 Importantly, hydrologists have long been aware that the water storage effects were going to be important for  
374 understanding water cycle variability (e.g., Milly and Dunne, 2002b; Zhang et al., 2008; Donohue et al., 2010;  
375 Wang and Alimohammadi, 2012), but without readily available databases it has been difficult to quantify water  
376 cycle variability in a consistent way. For example, we are not aware of maps showing global spatial patterns in  
377 variance for any terms of the water balance (except for  $P$ ). In this study, we have used a recently released global



378 gridded hydrologic re-analysis product, i.e., the Climate Data Record (CDR) to conduct an initial investigation of  
379 inter-annual variability in the terrestrial branch of the global water cycle. To the best of our knowledge, the results  
380 in our manuscript present the first attempt to gain a global overview of the magnitude for various terms (Eq. 2)  
381 that document variability in the water cycle. Our results demonstrate that the global patterns of inter-annual  
382 variability in the water cycle do not simply follow those of the long-term mean. In particular, with the variance  
383 calculations, the annual anomalies are squared and hence do not cancel out (like they do when calculating the  
384 mean). Hence we were initially surprised that the inter-annual variability of water storage change ( $\sigma_{\Delta S}^2$ ) is typically  
385 larger than the inter-annual variability of evapotranspiration ( $\sigma_E^2$ ). Moreover, the covariance components are also  
386 prominent and can be negative, which means that it is possible for the variability in the sinks (e.g.,  $\sigma_Q^2$ ,  $\sigma_{\Delta S}^2$ ) can  
387 actually exceed the variability in the source ( $\sigma_P^2$ ) (Eq. 2).

388

389 Our further analysis based on six climate end members, dry/wet, high/low water storage capacity and hot/cold  
390 offered some further general insights about hydrologic variability. For example, under extremely dry (water-  
391 limited) conditions, with limited storage capacity ( $S_{\max}$ ) we found that  $E$  follows  $P$  and  $\sigma_E^2$  follows  $\sigma_P^2$ , with  $\sigma_Q^2$   
392 and  $\sigma_{\Delta S}^2$  approaching zero. However, as  $S_{\max}$  increases, the partitioning of  $\sigma_P^2$  progressively shifts to a balance  
393 between  $\sigma_E^2$ ,  $\sigma_{\Delta S}^2$  and  $\text{cov}(E, \Delta S)$  (Fig. 12-14). Under extremely wet (energy-limited) and hot environments (i.e.,  
394 no snow/ice impact) we found the inter-annual variations in  $P$  mostly be partitioned to inter-annual variations in  
395  $Q$  (with both  $\sigma_E^2$  and  $\sigma_{\Delta S}^2$  approaching zero). However, in wet environments that were cold, we expected thermal  
396 processes (freeze/melt) to play a critical role in the hydrologic variability. Our results confirm that, with the  
397 finding that hydrologic partitioning of variability was highly (spatially) variable under extremely cold conditions  
398 (Fig. 12-14) and we were unable to provide any useful simplifications to summarise the data. These results  
399 highlight a key point that while the long-term mean state is not especially sensitive to variations in hydrologic  
400 water storage or phase, the long-term variability is very sensitive to those same variations.

401

402 The most complex results were found in semi-arid/semi-humid ( $0.5 < \overline{E_o}/\overline{P} < 1.5$ ) environments, where all three  
403 covariances (Eq. 2) were found to play critical roles in the overall partitioning of variability (Figs. 4-5). In many  
404 regions, the (absolute) magnitudes of the covariances were actually larger than the variances of the water balance  
405 components  $E$ ,  $Q$  and  $\Delta S$  (e.g., Fig. 8). That result demonstrates that deeper understanding of the process-level  
406 interactions that are embedded within each of the three covariance terms is still needed to help understand  
407 variability in the water cycle in these biologically productive regions ( $0.5 < \overline{E_o}/\overline{P} < 1.5$ ).



408

409 This study should be viewed as an initial investigation of the inter-annual variability in the global land water cycle.

410 We managed to obtain some syntheses based on the availability of current data, and we expect that with the

411 improvement of hydrologic databases over the coming years some of the detailed spatial patterns may change.

412 However, even from this initial investigation, some general principles do already appear clear. One general finding

413 is that the global pattern in the partitioning of inter-annual variability in the water cycle is not simply a reflection

414 of patterns in the partitioning of the long-term mean. For example, while the inter-annual water storage change is

415 often (safely) assumed to be negligible in terms of the long-term mean state, it is clear that storage variations are

416 central to understanding inter-annual variability of global water cycle. A second generalisation is that the

417 covariance components (Eq. 2) can be relatively large and are negative in some regions. The consequence is that

418 variability in the sinks (e.g.,  $\sigma_Q^2$ ,  $\sigma_{\Delta S}^2$ ) can, and do, exceed the variability in the source ( $\sigma_P^2$ ), especially in

419 biologically productive regions (Fig. 4).

420

421 The syntheses of the long-term mean water cycle originated in 1970s (Budyko, 1974), and it took several decades

422 for those general principles to become widely adopted in the hydrologic community. It remains a challenge to

423 develop a synthesis of hydro-climatic variability in the terrestrial branch of the water cycle, and major intellectual

424 efforts will be needed to develop generally applicable principles.

425

426 **6. Conclusions**

427

428 In this study, we describe an initial investigation of the inter-annual variability of the terrestrial branch in the

429 global water cycle that uses the recently released global monthly Climate Data Record (CDR) database for  $P$ ,  $E$ ,430  $Q$  and  $\Delta S$ . We start by investigating the partitioning of  $P$  in the water cycle in terms of long-term mean and then431 extend that to the inter-annual variability. While the mean annual  $P$  is mostly partitioned into mean annual  $E$  and432  $Q$ , as is well known. However, we find that the variance of  $P$  ( $\sigma_P^2$ ) is mostly partitioned into the variance of  $Q$  ( $\sigma_Q^2$ )433 and variance of  $\Delta S$  ( $\sigma_{\Delta S}^2$ ). This result indicates that the global patterns of inter-annual variability in the water cycle

434 do not simply follow the long-term mean. A second general finding is that the covariance components are

435 important and can be negative in some regions, indicating the variability in the sinks (e.g.,  $\sigma_Q^2$ ,  $\sigma_{\Delta S}^2$ ) can, and do,436 exceed the variability in the source ( $\sigma_P^2$ ). Our attempts to develop deeper understanding of variance partitioning

437 led to some syntheses in extreme environments (wet/dry vs hot/cold). In particular, we find that in extremely dry



438 environments (either hot/cold) the partitioning of  $\sigma_p^2$  is closely related to the water storage capacity. With limited  
439 storage capacity, the partitioning of  $\sigma_p^2$  is mostly to  $\sigma_E^2$  but as the storage capacity increases, the partitioning of  
440  $\sigma_p^2$  is increasingly shared between  $\sigma_E^2$  and  $\sigma_{\Delta S}^2$  and the covariance between those variables (Fig. 14). In contrast,  
441 in extremely wet environments, there are large divergences in the variance partitioning between hot and cold  
442 conditions. In hot conditions,  $\sigma_p^2$  is mostly partitioned to  $\sigma_Q^2$  but under cold conditions,  $\sigma_p^2$  is partitioned to all  
443 available variability sinks (Fig. 14). However, in biologically productive semi-arid/semi-humid ( $0.5 < \overline{E_o}/\overline{P} < 1.5$ )  
444 environments, we found the variance partitioning to be very complex and that partitioning was not obviously  
445 associated with simple environmental factors. A general understanding of hydro-climatic variability remains a  
446 major intellectual challenge and we anticipate major efforts will be needed to synthesise general principles that  
447 cover the full spectrum of hydrologic variability.

448

#### 449 **Acknowledgements**

450 This research was supported by the Australian Research Council (CE11E0098, CE170100023), and D.Y.  
451 acknowledges support by the National Natural Science Foundation of China (51609122). The authors declare that  
452 there is no conflict of interests regarding the publication of this paper. All data used in this paper are available  
453 online as referenced in the 'Methods and Data' section.

454

#### 455 **References**

- 456 Agarwal, D. A., Humphrey, M., Beekwilder, N. F., Jackson, K. R., Goode, M. M., and van Ingen, C.: A data-centered  
457 collaboration portal to support global carbon-flux analysis, *Concurr. Comp-Pract. E.*, 22, 2323-2334,  
458 <https://doi.org/10.1002/cpe.1600>, 2010.
- 459 Baldocchi, D., Falge, E., Gu, L., Olson, R., Hollinger, D., Running, S., Anthoni, P., Bernhofer, C., Davis, K., Evans, R.,  
460 Fuentes, J., Goldstein, A., Katul, G., Law, B., Lee, X., Malhi, Y., Meyers, T., Munger, W., Oechel, W., Paw U, K. T.,  
461 Pilegaard, K., Schmid, H. P., Valentini, R., Verma, S., Vesala, T., Wilson, K., and Wofsy, S.: FLUXNET: A New Tool  
462 to Study the Temporal and Spatial Variability of Ecosystem-Scale Carbon Dioxide, Water Vapor, and Energy Flux  
463 Densities, *B. Am. Meteorol. Soc.*, 82, 2415-2434, [https://doi.org/10.1175/1520-0477\(2001\)082<2415:FANTTS>2.3.CO;2](https://doi.org/10.1175/1520-0477(2001)082<2415:FANTTS>2.3.CO;2), 2001.
- 465 Budyko, M. I.: *Climate and Life*. Academic Press, London, 1974.





- 466 Choudhury, B. J.: Evaluation of an empirical equation for annual evaporation using field observations and results  
467 from a biophysical model, *J. Hydrol.*, 216, 99-110, [https://doi.org/10.1016/S0022-1694\(98\)00293-5](https://doi.org/10.1016/S0022-1694(98)00293-5), 1999.
- 468 Dee, D. P., Uppala, S. M., Simmons, A. J., Berrisford, P., Poli, P., Kobayashi, S., Andrae, U., Balmaseda, M. A.,  
469 Balsamo, G., Bauer, P., Bechtold, P., Beljaars, A. C. M., van de Berg, L., Bidlot, J., Bormann, N., Delsol, C., Dragani,  
470 R., Fuentes, M., Geer, A. J., Haimberger, L., Healy, S. B., Hersbach, H., Hólm, E. V., Isaksen, I., Kållberg, P., Köhler,  
471 M., Matricardi, M., McNally, A. P., Monge-Sanz, B. M., Morcrette, J. J., Park, B. K., Peubey, C., de Rosnay, P.,  
472 Tavolato, C., Thépaut, J. N., and Vitart, F.: The ERA-Interim reanalysis: configuration and performance of the  
473 data assimilation system, *Q. J. R. Meteorol. Soc.*, 137, 553-597, <https://doi.org/10.1002/qj.828>, 2011.
- 474 Donohue, R. J., Roderick, M. L., and McVicar, T. R.: Can dynamic vegetation information improve the accuracy of  
475 Budyko's hydrological model?, *J. Hydrol.*, 390, 23-34, <https://doi.org/10.1016/j.jhydrol.2010.06.025>, 2010.
- 476 Fu, B. P.: On the Calculation of the Evaporation from Land Surface, *Sci. Atmos. Sin.*, 5, 23-31, 1981.
- 477 Harris, I., Jones, P. D., Osborn, T. J., and Lister, D. H.: Updated high-resolution grids of monthly climatic  
478 observations—the CRU TS3.10 Dataset, *Int. J. Climatol.*, 34, 623-642, <https://doi.org/10.1002/joc.3711>, 2014.
- 479 Huning, L. S., and AghaKouchak, A.: Mountain snowpack response to different levels of warming, *Proc. Natl.*  
480 *Acad. Sci. U. S. A.*, 115, 10932, <https://doi.org/10.1073/pnas.1805953115>, 2018.
- 481 Jackson, R. B., Canadell, J., Ehleringer, J. R., Mooney, H. A., Sala, O. E., and Schulze, E. D.: A Global Analysis of  
482 Root Distributions for Terrestrial Biomes, *Oecologia*, 108, 389-411, <https://doi.org/10.1007/BF00333714>, 1996.
- 483 Jung, M., Reichstein, M., Ciais, P., Seneviratne, S. I., Sheffield, J., Goulden, M. L., Bonan, G., Cescatti, A., Chen, J.,  
484 de Jeu, R., Dolman, A. J., Eugster, W., Gerten, D., Gianelle, D., Gobron, N., Heinke, J., Kimball, J., Law, B. E.,  
485 Montagnani, L., Mu, Q., Mueller, B., Oleson, K., Papale, D., Richardson, A. D., Rouspard, O., Running, S., Tomelleri,  
486 E., Viovy, N., Weber, U., Williams, C., Wood, E., Zaehle, S., and Zhang, K.: Recent decline in the global land  
487 evapotranspiration trend due to limited moisture supply, *Nature*, 467, 951,  
488 <https://doi.org/10.1038/nature09396>, 2010.
- 489 Koster, R. D., and Suarez, M. J.: A Simple Framework for Examining the Interannual Variability of Land Surface  
490 Moisture Fluxes, *J. Clim.*, 12, 1911-1917, [https://doi.org/10.1175/1520-0442\(1999\)012<1911:ASFFET>2.0.CO;2](https://doi.org/10.1175/1520-0442(1999)012<1911:ASFFET>2.0.CO;2),  
491 1999.



- 492 McMahon, T. A., Peel, M. C., Pegram, G. G. S., and Smith, I. N.: A Simple Methodology for Estimating Mean and  
493 Variability of Annual Runoff and Reservoir Yield under Present and Future Climates, *J. Hydrometeorol.*, 12, 135-  
494 146, <https://doi.org/10.1175/2010jhm1288.1>, 2011.
- 495 Milly, P. C. D.: Climate, soil water storage, and the average annual water balance, *Water Resour. Res.*, 30, 2143-  
496 2156, <https://doi.org/10.1029/94WR00586>, 1994a.
- 497 Milly, P. C. D.: Climate, interseasonal storage of soil water, and the annual water balance, *Adv. Water Resour.*,  
498 17, 19-24, [https://doi.org/10.1016/0309-1708\(94\)90020-5](https://doi.org/10.1016/0309-1708(94)90020-5), 1994b.
- 499 Milly, P. C. D., and Dunne, K. A.: Macroscale water fluxes 1. Quantifying errors in the estimation of basin mean  
500 precipitation, *Water Resour. Res.*, 38, 23-21-23-14, <https://doi.org/10.1029/2001WR000759>, 2002a.
- 501 Milly, P. C. D., and Dunne, K. A.: Macroscale water fluxes 2. Water and energy supply control of their interannual  
502 variability, *Water Resour. Res.*, 38, 24-21-24-29, <https://doi.org/10.1029/2001WR000760>, 2002b.
- 503 Mueller, B., Hirschi, M., Jimenez, C., Ciais, P., Dirmeyer, P. A., Dolman, A. J., Fisher, J. B., Jung, M., Ludwig, F.,  
504 Maignan, F., Miralles, D. G., McCabe, M. F., Reichstein, M., Sheffield, J., Wang, K., Wood, E. F., Zhang, Y., and  
505 Seneviratne, S. I.: Benchmark products for land evapotranspiration: LandFlux-EVAL multi-data set synthesis,  
506 *Hydrol. Earth. Syst. Sci.*, 17, 3707-3720, <https://doi.org/10.5194/hess-17-3707-2013>, 2013.
- 507 Norby, R. J., Ledford, J., Reilly, C. D., Miller, N. E., and O'Neill, E. G.: Fine-root production dominates response of  
508 a deciduous forest to atmospheric CO<sub>2</sub> enrichment, *Proc. Natl. Acad. Sci. U. S. A.*, 101, 9689-9693,  
509 <https://doi.org/10.1073/pnas.0403491101>, 2004.
- 510 Rodell, M., Beaudoing, H. K., L'Ecuyer, T. S., Olson, W. S., Famiglietti, J. S., Houser, P. R., Adler, R., Bosilovich, M.  
511 G., Clayson, C. A., Chambers, D., Clark, E., Fetzer, E. J., Gao, X., Gu, G., Hilburn, K., Huffman, G. J., Lettenmaier,  
512 D. P., Liu, W. T., Robertson, F. R., Schlosser, C. A., Sheffield, J., and Wood, E. F.: The Observed State of the Water  
513 Cycle in the Early Twenty-First Century, *J. Clim.*, 28, 8289-8318, <https://doi.org/10.1175/JCLI-D-14-00555.1>,  
514 2015.
- 515 Roderick, M. L., and Farquhar, G. D.: A simple framework for relating variations in runoff to variations in climatic  
516 conditions and catchment properties, *Water Resour. Res.*, 47, <https://doi.org/10.1029/2010WR009826>, 2011.
- 517 Sankarasubramanian, A., and Vogel, R. M.: Annual hydroclimatology of the United States, *Water Resour. Res.*,  
518 38, 19-11-19-12, <https://doi.org/10.1029/2001WR000619>, 2002.
- 519 Scanlon, B. R., Zhang, Z., Save, H., Sun, A. Y., Müller Schmied, H., van Beek, L. P. H., Wiese, D. N., Wada, Y., Long,  
520 D., Reedy, R. C., Longuevergne, L., Döll, P., and Bierkens, M. F. P.: Global models underestimate large decadal



- 521 declining and rising water storage trends relative to GRACE satellite data, Proc. Natl. Acad. Sci. U. S. A.,  
522 <https://doi.org/10.1073/pnas.1704665115>, 2018.
- 523 Sposito, G.: Understanding the Budyko Equation, Water, 9, <https://doi.org/10.3390/w9040236>, 2017.
- 524 Stackhouse, P. W., Gupta, S. K., Cox, S. J., Mikovitz, J. C., Zhang, T., and Hinkelman, L. M.: The NASA/GEWEX  
525 Surface Radiation Budget Release 3.0: 24.5-Year Dataset. In: GEWEX News, No. 1, 2011.
- 526 Ukkola, A. M., Haughton, N., De Kauwe, M. G., Abramowitz, G., and Pitman, A. J.: FluxnetLSM R package (v1.0):  
527 a community tool for processing FLUXNET data for use in land surface modelling, Geosci. Model. Dev., 10, 3379-  
528 3390, <https://doi.org/10.5194/gmd-10-3379-2017>, 2017.
- 529 Wang, D., and Alimohammadi, N.: Responses of annual runoff, evaporation, and storage change to climate  
530 variability at the watershed scale, Water Resour. Res., 48, <https://doi.org/10.1029/2011WR011444>, 2012.
- 531 Wang-Erlandsson, L., Bastiaanssen, W. G. M., Gao, H., Jägermeyr, J., Senay, G. B., van Dijk, A. I. J. M., Guerschman,  
532 J. P., Keys, P. W., Gordon, L. J., and Savenije, H. H. G.: Global root zone storage capacity from satellite-based  
533 evaporation, Hydrol. Earth Syst. Sci., 20, 1459-1481, <https://doi.org/10.5194/hess-2015-533>, 2016.
- 534 Yang, H., Yang, D., Lei, Z., and Sun, F.: New analytical derivation of the mean annual water-energy balance  
535 equation, Water Resour. Res., 44, <https://doi.org/10.1029/2007WR006135>, 2008.
- 536 Yang, Y., Donohue, R. J., and McVicar, T. R.: Global estimation of effective plant rooting depth: Implications for  
537 hydrological modeling, Water Resour. Res., 52, 8260-8276, <https://doi.org/10.1002/2016WR019392>, 2016.
- 538 Zeng, R., and Cai, X.: Assessing the temporal variance of evapotranspiration considering climate and catchment  
539 storage factors, Adv. Water Resour., 79, 51-60, <https://doi.org/10.1016/j.advwatres.2015.02.008>, 2015.
- 540 Zhang, L., Potter, N., Hickel, K., Zhang, Y., and Shao, Q.: Water balance modeling over variable time scales based  
541 on the Budyko framework – Model development and testing, J. Hydrol., 360, 117-131,  
542 <https://doi.org/10.1016/j.jhydrol.2008.07.021>, 2008.
- 543 Zhang, Y., Pan, M., Sheffield, J., Siemann, A. L., Fisher, C. K., Liang, M. L., Beck, H. E., Wanders, N., MacCracken,  
544 R. F., Houser, P. R., Zhou, T., Lettenmaier, D. P., Ma, Y., Pinker, R. T., Bytheway, J., Kummerow, C. D., and Wood,  
545 E. F.: A Climate Data Record (CDR) for the global terrestrial water budget: 1984-2010, Hydrol. Earth Syst. Sci., 22,  
546 241-263, <https://doi.org/10.5194/hess-22-241-2018>, 2018.
- 547
- 548

549 **List of Figures:**

550 Figure 1. Spatial mask used in this study.

551 Figure 2. Mean annual (1984-2010) (a)  $P$ , (b)  $E$  and (c)  $Q$ .552 Figure 3. Relationship of mean annual (a) evapotranspiration ( $\bar{E}/\bar{P}$ ) and (b) runoff ( $\bar{Q}/\bar{P}$ ) ratios to the aridity  
553 index ( $\bar{E}_o/\bar{P}$ ) from the CDR and SRB databases.554 Figure 4. Water cycle variances ( $\sigma_P^2$ ,  $\sigma_E^2$ ,  $\sigma_Q^2$ ,  $\sigma_{\Delta S}^2$ ) and covariances ( $cov(E, Q)$ ,  $cov(E, \Delta S)$ ,  $cov(Q, \Delta S)$ ).555 Figure 5. Distribution of water cycle variances ( $\sigma_P^2$ ,  $\sigma_E^2$ ,  $\sigma_Q^2$ ,  $\sigma_{\Delta S}^2$ ) and covariances ( $cov(E, Q)$ ,  $cov(E, \Delta S)$ ,  
556  $cov(Q, \Delta S)$ ).557 Figure 6. Relation between inter-annual mean and standard deviation for (a)  $P$ , (b)  $E$  and (c)  $Q$  from the CDR  
558 database.559 Figure 7. Relationship of inter-annual standard deviation of (a) evapotranspiration ( $\sigma_E/\sigma_P$ ) and (b) runoff ( $\sigma_Q/\sigma_P$ )  
560 ratios to aridity ( $\bar{E}_o/\bar{P}$ ).561 Figure 8. Relation between water cycle variances-covariances (see Fig. 4b-g) as a fraction of the variance of  $P$   
562 ( $\sigma_P^2$ ) and the aridity index ( $\bar{E}_o/\bar{P}$ ) coloured by density.563 Figure 9. Relation between water cycle variances-covariances (see Fig. 4b-g) as a fraction of the variance for  $P$   
564 ( $\sigma_P^2$ ) and the aridity index ( $\bar{E}_o/\bar{P}$ ) for grid-cells over different latitude ranges (i.e., 90N-60N, 60N-30N, 30N-0  
565 and 0-90S). The colours relate to the water storage capacity  $S_{\max}$ .566 Figure 10. Relation between water cycle variances-covariances (see Fig. 4b-g) as a fraction of the variance for  $P$   
567 ( $\sigma_P^2$ ) and the aridity index ( $\bar{E}_o/\bar{P}$ ) for grid-cells over different latitude ranges (i.e., 90N-60N, 60N-30N, 30N-0  
568 and 0-90S). The colours relate to the mean air temperature ( $\bar{T}_a$ ).

569 Figure 11. Locations of three representative grid-cells used as case study sites.

570 Figure 12. Inter-annual time series ( $P$ ,  $E$ ,  $Q$  and  $\Delta S$ ) and the associated variance-covariance matrix ( $E$ ,  $Q$  and  $\Delta S$ )  
571 for case study Sites 1-3.

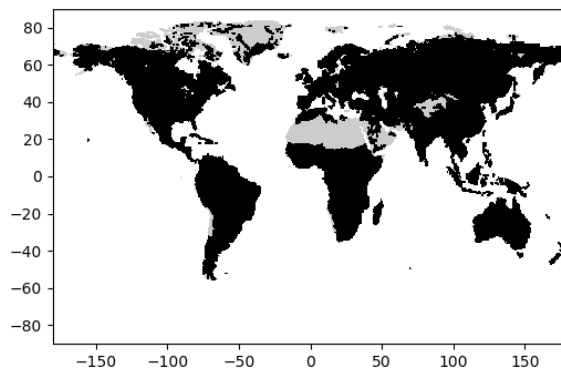
572 Figure 13. Location of three case study sites in the water cycle variability space.

573 Figure 14. Synthesis of factors controlling variance partitioning.

574



575



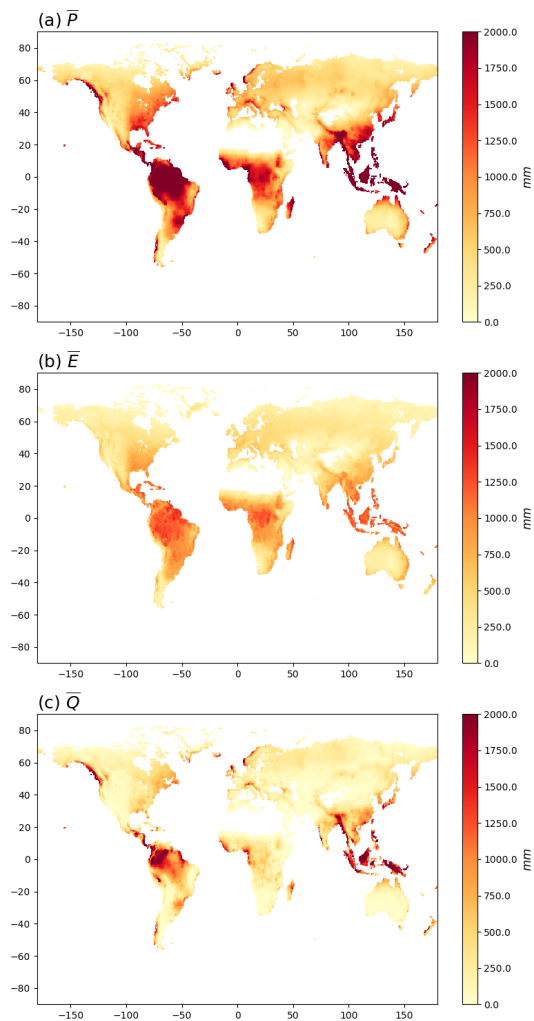
576

577 **Figure 1. Spatial mask used in this study. Grey areas (Himalayan region, Sahara Desert, Greenland) have been**  
578 **masked out of the CDR database.**

579



580



581

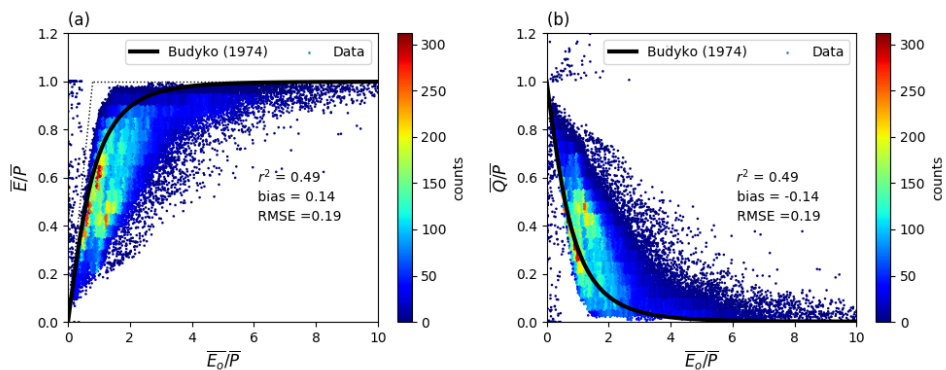
582 **Figure 2. Mean annual (1984-2010) (a)  $P$ , (b)  $E$  and (c)  $Q$ . Note that the mean annual  $\Delta S$  in the CDR database is zero**

583 **by construction and is not shown.**

584



585



586

587 **Figure 3. Relationship of mean annual (a) evapotranspiration ( $\bar{E}/\bar{P}$ ) and (b) runoff ( $\bar{Q}/\bar{P}$ ) ratios to the aridity index**

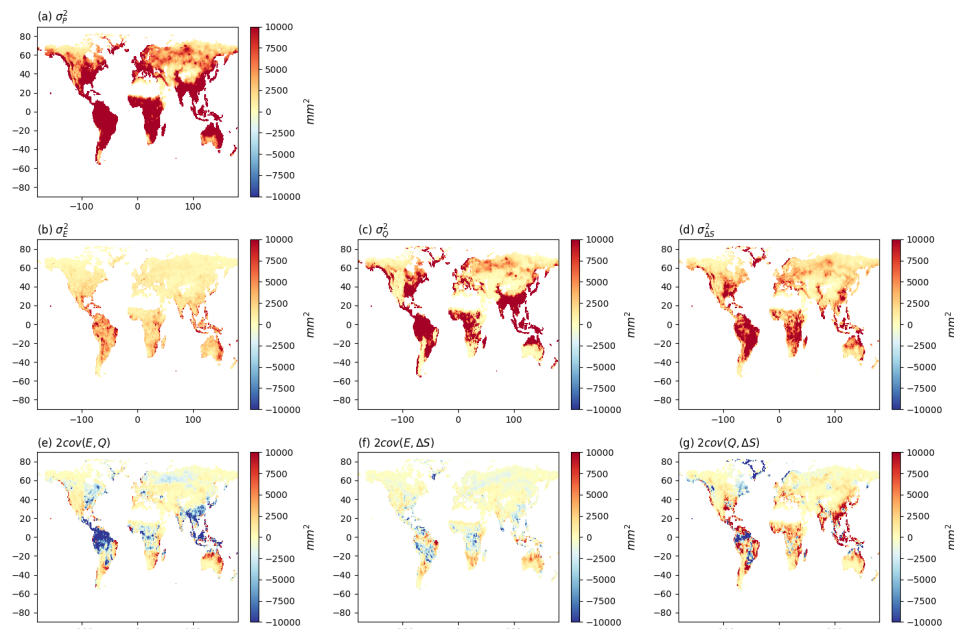
588 **( $\bar{E}_0/\bar{P}$ ) from the CDR and SRB databases. For comparison, the Budyko (1974) curve is shown on the left panel (Fig.**

589 **3a). The curve on the right panel (Fig. 3b) is calculated assuming a steady state ( $\bar{Q}/\bar{P} = 1 - \bar{E}/\bar{P}$ ).**

590



591



592

593 **Figure 4. Water cycle variances ( $\sigma_P^2$ ,  $\sigma_E^2$ ,  $\sigma_Q^2$ ,  $\sigma_{\Delta S}^2$ ) and covariances ( $cov(E, Q)$ ,  $cov(E, \Delta S)$ ,  $cov(Q, \Delta S)$ ). Note that we**

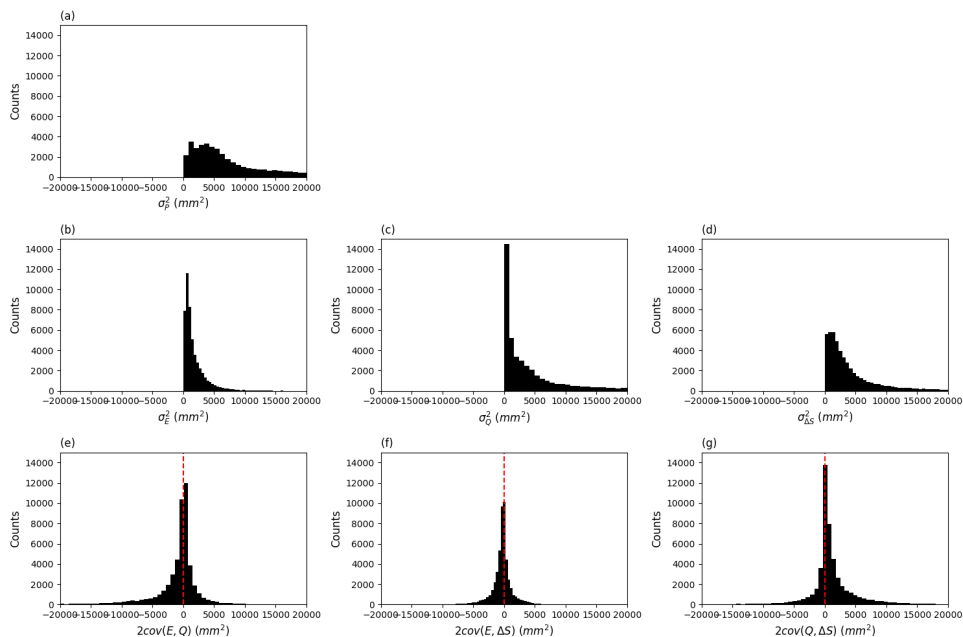
594 **have multiplied the covariances by two (see Eq. 2).**

595





596



597

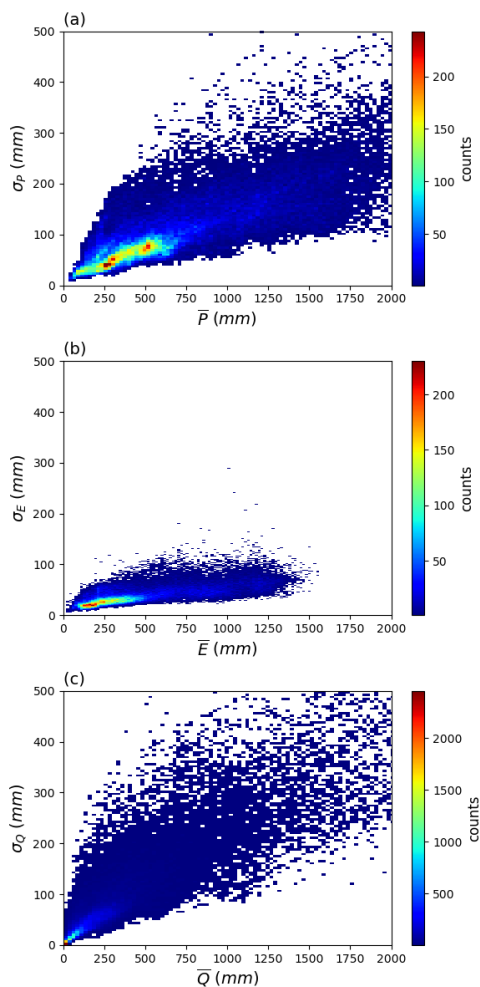
598 **Figure 5.** Distribution of water cycle variances ( $\sigma_p^2, \sigma_E^2, \sigma_Q^2, \sigma_{\Delta S}^2$ ) and covariances ( $cov(E, Q), cov(E, \Delta S), cov(Q, \Delta S)$ ).

599 Note that we have multiplied the covariances by two (see Eq. 2).

600



601



602

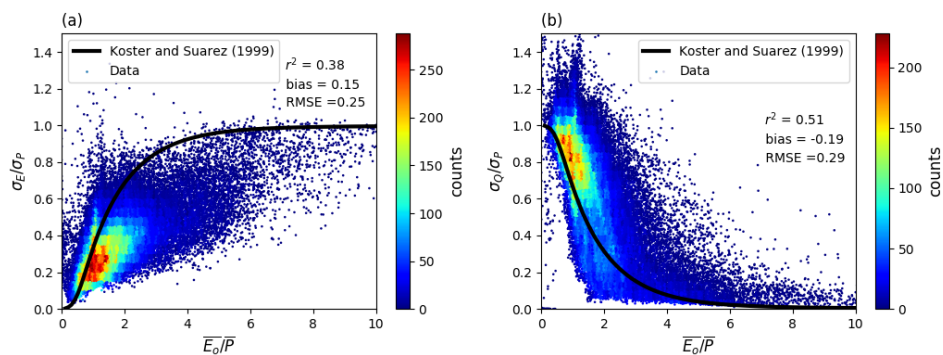
603 **Figure 6. Relation between inter-annual mean and standard deviation for (a)  $P$ , (b)  $E$  and (c)  $Q$  from the CDR**

604 **database. Note that the mean annual  $\Delta S$  is zero by construction and is not shown.**

605



606



607

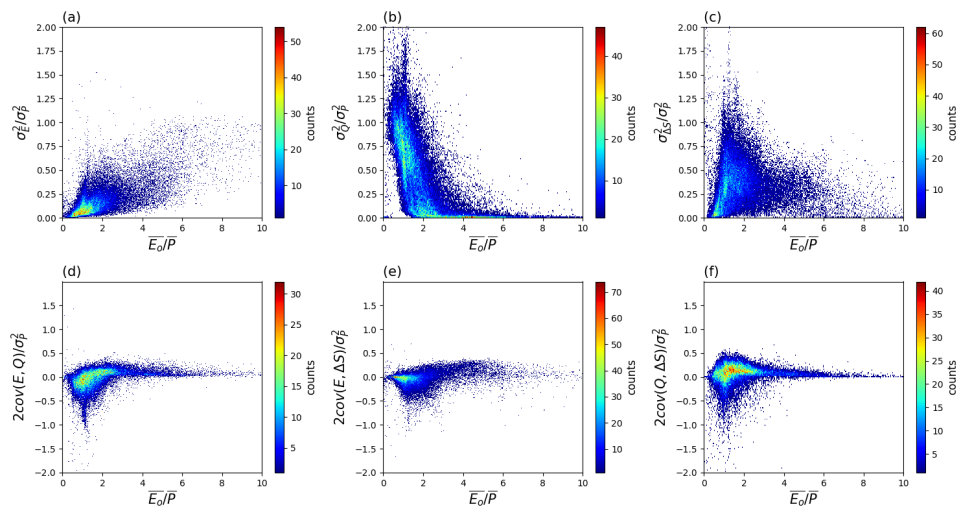
608 **Figure 7. Relationship of inter-annual standard deviation of (a) evapotranspiration ( $\sigma_E/\sigma_P$ ) and (b) runoff ( $\sigma_Q/\sigma_P$ )**

609 **ratios to aridity ( $\overline{E_o}/\overline{P}$ ). The curves represent the semi-empirical relations from Koster and Suarez (1999).**

610



611



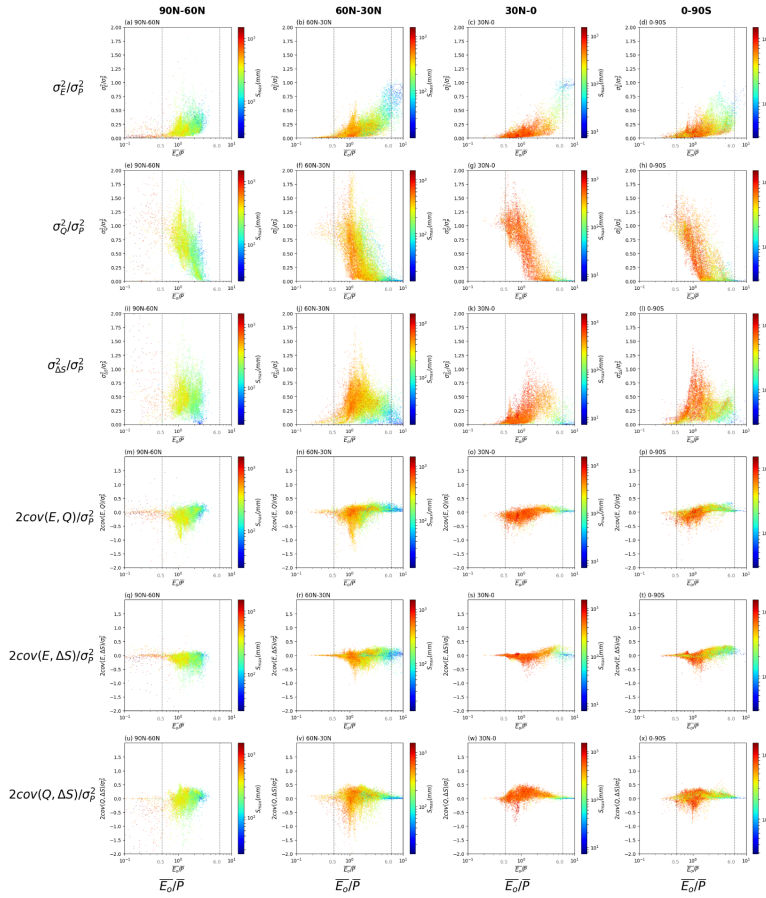
612

613 **Figure 8.** Relation between water cycle variances-covariances (see Fig. 4b-g) as a fraction of the variance of  $P$  ( $\sigma_P^2$ ) and  
 614 the aridity index ( $\bar{E}_O/\bar{P}$ ) coloured by density. Note that we have multiplied the covariance components by two (see Eq.  
 615 2).

616



617



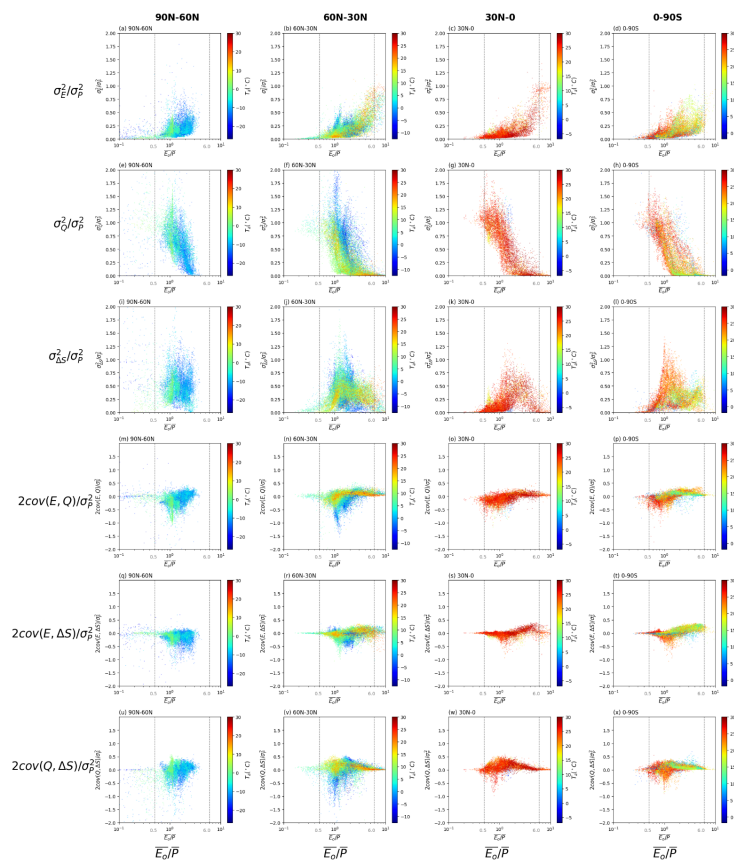
618

619 **Figure 9.** Relation between water cycle variances-covariances (see Fig. 4b-g) as a fraction of the variance for  $P$  ( $\sigma_P^2$ )  
 620 and the aridity index ( $\overline{E_0}/\overline{P}$ ) for grid-cells over different latitude ranges (i.e., 90N-60N, 60N-30N, 30N-0 and 0-90S).  
 621 The colours relate to the water storage capacity  $S_{\max}$ . Note that we have multiplied the covariances by two (see Eq. 2).  
 622 The vertical grey dashed lines represent thresholds used to separate extremely dry ( $\overline{E_0}/\overline{P} \geq 6.0$ ) and wet ( $\overline{E_0}/\overline{P} \leq 0.5$ )  
 623 environments. Note the use of a logarithmic x-axis and scale bar for  $S_{\max}$ .

624



625



626

627 **Figure 10.** Relation between water cycle variances-covariances (see Fig. 4b-g) as a fraction of the variance for  $P$  ( $\sigma_P^2$ )

628 and the aridity index ( $\overline{E_0/P}$ ) for grid-cells over different latitude ranges (i.e., 90N-60N, 60N-30N, 30N-0 and 0-90S).

629 The colours relate to the mean air temperature ( $\overline{T_a}$ ). Note that we have multiplied the covariances by two (see Eq. 2).

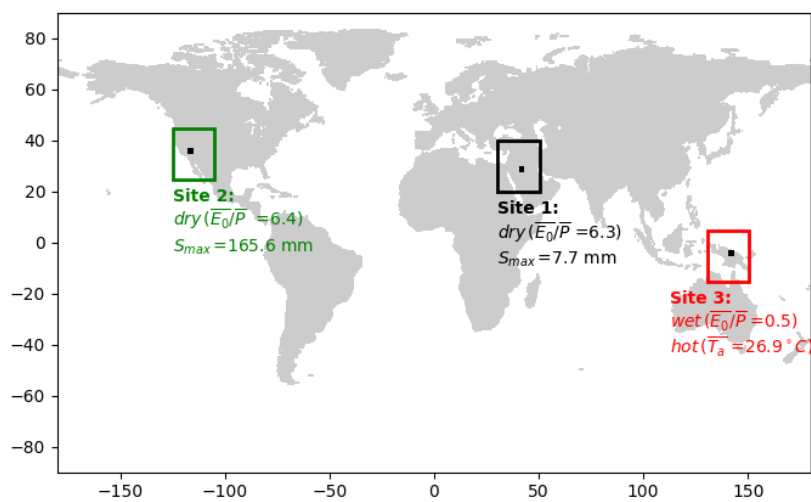
630 The vertical grey dashed lines represent thresholds used to separate extremely dry ( $\overline{E_0/P} \geq 6.0$ ) and wet ( $\overline{E_0/P} \leq$

631 0.5) environments.

632



633



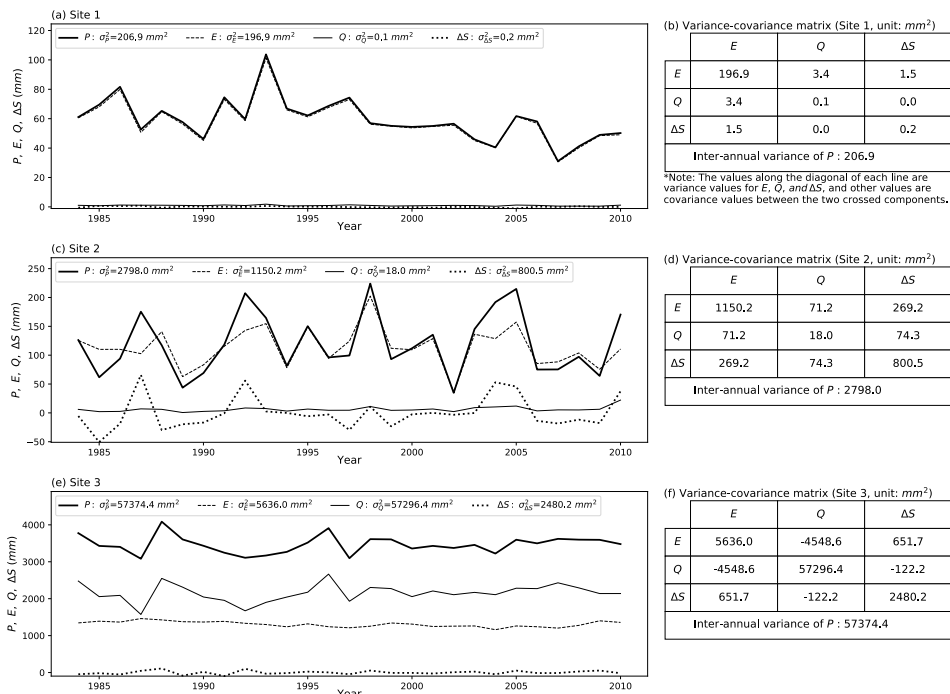
634

635 **Figure 11.** Locations of three representative grid-cells used as case study sites.

636



637



638

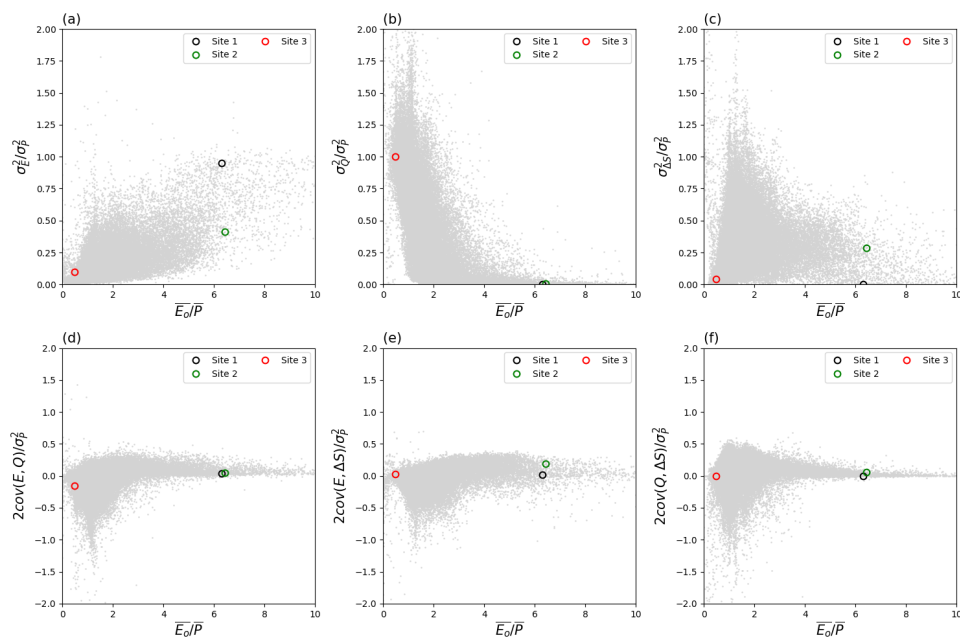
639 **Figure 12. Inter-annual time series ( $P$ ,  $E$ ,  $Q$  and  $\Delta S$ ) and the associated variance-covariance matrix ( $E$ ,  $Q$  and  $\Delta S$ ) for**  
 640 **case study Sites 1-3. Left column shows time series for (a) Site 1, (c) Site 2 and (e) Site 3, with right column i.e., (b), (d)**  
 641 **and (f), the associated variance-covariance matrix for three sites. Note that the covariance values in the tables should**  
 642 **be multiplied by two to agree with the variance-covariance balance in Eq. (2).**

643





644



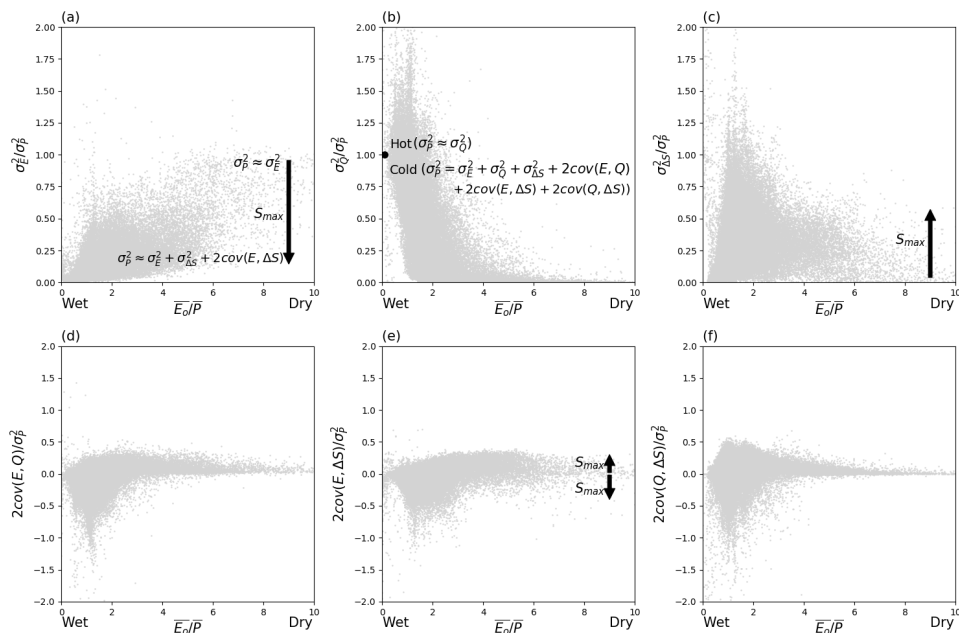
645

646 **Figure 13.** Location of three case study sites in the water cycle variability space. The grey background dots are from  
647 **Fig. 8.**

648



649



650

651 **Figure 14. Synthesis of factors controlling variance partitioning. The arrows denote trends with increasing  $S_{max}$ . The**  
 652 **grey background dots are from Fig. 8.**

653